Available online at www.sciencedirect.com
SCIENCE DIRECT
ELSEVIER
Colloids and Surfaces A: Physicochem. Eng. Aspects 267 (2005) 86–94
COLLOIDS AND SURFACES A
www.elsevier.com/locate/colsurfa

Flow imaging of dilute colloidal suspension in PDMS-based microfluidic chip using fluorescence microscopy

Myung-Suk Chun *, Sangwoo Lee [1]

Complex Fluids Research Lab., Korea Institute of Science and Technology (KIST), P.O. Box 131, Cheongryang, Seoul 130–650, South Korea

Available online 3 August 2005

Abstract

A slit-like flow channel was designed to allow for fluorescent microscope visualization in the microfluidic chip fabricated with glass substrate and polydimethylsiloxane (PDMS). For the exposure time, moving fluorescent polystyrene latexes of 1 μm radius result in image streaks, where the latex concentration is sufficiently dilute underlying the condition of simple fluid. Applying the data processing method for particle streak imaging developed ourselves, the linear velocity of particle at the lateral position of the channel was determined in terms of a ratio of the real distance to the number of pixels. It is obvious that the velocity profile of suspension depends on the surface properties of the microchannel wall. The reliability of the velocity profile determined by the flow imaging is justified by comparing with the measured volumetric flow rate. We recognized the behavior of fluid slip in velocity profiles at the hydrophobic surface of PDMS wall. The slip length inferred from the experimental results was evaluated ranging 6–8 μm.

Keywords: Particle streak; Microfluidic chip; Colloidal suspension; Slip velocity; Fluorescent microscope; Surface potential

1. Introduction

Microfluidic and nanofluidic devices perform various chip-based chemical and biological analyses. Flow imaging has played a central role in the emerging field of micro- and nanofluidics. Direct flow imaging is of key importance for the fundamental understanding of microflows, analyzing, evaluating and developing novel micro processes [1,2]. Further, it is necessary to investigate the non-ideal behavior such as spatial and temporal gradients in fluid and surface properties, which appears in miniaturized systems. Experimental observations provide reasonably benchmark data for the verification of attempting theoretical study.

In particle-based flow velocimetry, the motion of the bulk fluid is inferred from the observed velocity of marker particles [3]. Note that different methods of acquiring and analyzing the particle data have evolved especially including particle streak velocimetry (PSV) and particle image velocimetry (PIV) [4–7]. The PSV adopted in this study involves recording particle displacements in a single image over a period of time, in which sparse quantitative particle velocity data may be obtained.

Earlier particle-based measurements in electrokinetic flows include the work done with particle streak images and simple convolution studies. Taylor and Yeung [8] applied streak imaging of fluorescent sub-micron particles in both electrokinetically and pressure-driven flows. The length and direction of the streaks were used to infer the vector velocity field and thus to obtain velocity profiles. A general parabolic profile was displayed in the pressure-driven flow. For an electroosmotic flow, they observed a small velocity defect in the center of the capillary and attributed it to particle-induced viscous drag on the flow. More recent works were reported, where the streak imaging has also been applied to quantify flow in an electric field free region [9,10]. Oddy et al. [11] visualized flow instabilities in an electrokinetic flow using particle streaking, where the streak images clearly depict the nature of the flow.

* Tel.: +82 2 958 5363; fax: +82 2 958 5205.
E-mail address: mschun@kist.re.kr (M.-S. Chun).
[1] Present address: Chemical Engineering and Materials Science Department, University of Minnesota, Minneapolis, MN55455, USA.

0927-7757/$ – see front matter © 2005 Elsevier B.V. All rights reserved.
doi:10.1016/j.colsurfa.2005.06.046

Nomenclature

d_p	diameter of particle (m)
E_z	applied electric field in axial direction (V/m)
e	elementary charge (C)
$\boldsymbol{G}$	$n \times m$ matrix for green color intensity (−)
$\boldsymbol{G}'_{L(ij)}$	local matrix including nine elements around g'_{ij} (−)
$\boldsymbol{G}'_{N,z}$	new noise-reduced matrix of $\boldsymbol{G}'_z$(−)
$\boldsymbol{G}'_z$	differentiation matrix of $\boldsymbol{G}$ in z direction (–)
g_{ij}	element of $\boldsymbol{G}$, or green color intensity for each pixel (−)
g'_{ij}	element of $\boldsymbol{G}'_{L(ij)}$ (–)
g_{max}	maximum point of $\boldsymbol{G}'_{N,z}$ (–)
g_{min}	minimum point of $\boldsymbol{G}'_{N,z}$ (–)
$g'_{N(ij)}$	new noise-reduced point (–)
H	channel depth (m)
kT	Boltzmann thermal energy (J)
L	channel length (m)
n	number concentration of ion species (1/m^3)
P	pressure (Pa)
t_E	exposure time (s)
v_z	axial particle velocity (m/s)
W	channel width (m)
Y	y/W (–)
y	lateral position (m)
$\boldsymbol{Z}$	backward difference operator (–)
z	axial position (m)

Greek letters

β	slip coefficient or slip length (m)
γ	ratio of real distance to number of pixels (m)
ε	dielectric constant, or permittivity of the medium (C^2/J m)
η	fluid viscosity (Pa s)
κ	inverse EDL thickness (1/m)
ϕ	flow-induced streaming potential (V)
Ψ	dimensionless electric potential (–)
ψ	electric potential (V)

In the present study, we investigate the velocity profile of dilute suspension of latex colloids in polydimethylsiloxane (PDMS) based microfluidic chip applying the PSV. The slit-like channel has been fabricated by designing high aspect ratio of the channel depth to the width that practically allows a one-dimensional flow. An appropriate data processing method has been developed for the image acquisition. To guarantee the accuracy of our method, the volumetric flow rate estimated from the regressions on the velocity profile is compared with the measured volumetric flow rate.

The PDMS has been widely used in the microfluidics field as a micro-fabrication material due to its simple process and low cost when compared to traditional etching and bonding approaches [12]. The PDMS surface is hydrophobic whereas the glass one is hydrophilic, therefore, this inhomogeneous surface condition results in an asymmetric velocity profile in the PDMS-glass microfluidic chip. We explore the behavior of the Navier's fluid slip encountered in a hydrophobic PDMS wall with variations of the surface potential, hypothetically corresponding to the zeta potential measured by experiments. The effect of fluid slip is to increase the flow velocity at a given pressure gradient, which plays a contrary role to the electroviscous effect giving rise to a reduction in the flow.

2. Principle of image analysis and processing

An appropriate exposure time is applied to record the streaks resulting from the motion of particles in the flow channel. In general, the digital image data consist of each pixel equivalent to the intensity of the light [4,5,11], and every image is stored in the computer with three elementary colors; red, green, and blue. If the seed particle contains green fluorescent color, the background can be red from a sodium transmitted light of microscope and the blue color is filtered. Then, an image of particle streak can be represented by the image with green color alone. This separated streak image is expressed in the matrix form $\boldsymbol{G}$ for $n \times m$ pixels.

In order to determine the start and the end points of a streak, we differentiate the green color image with respect to a flow direction of the particle. As shown in Fig. 1, the particle flows in z-direction. Here, taking the backward difference operator $\boldsymbol{Z}$ provides a differentiation of $\boldsymbol{G}$, which can

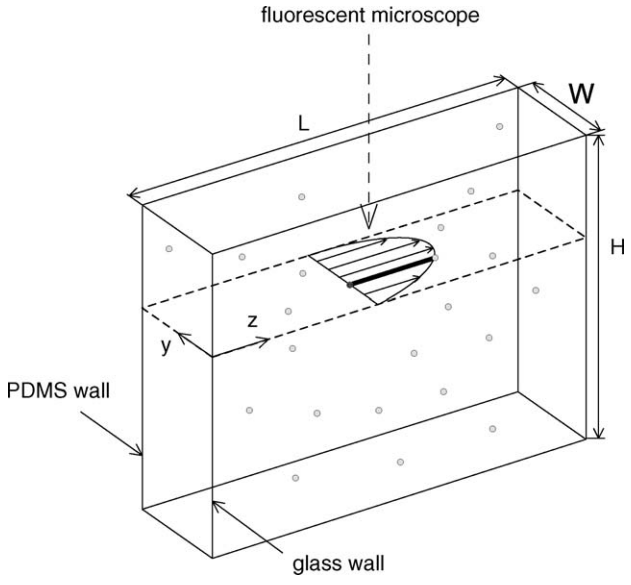

Fig. 1. Schematic volume containing the one-dimensional microflow of dilute colloidal suspension for particle streak imaging.

be written as

$$\boldsymbol{G}'_{\mathrm{z}} \equiv \boldsymbol{G}\boldsymbol{Z} = \begin{bmatrix} g_{1,1} & g_{1,2} & g_{1,3} & \cdots & g_{1,m-1} & g_{1,m} \\ g_{2,1} & g_{2,2} & g_{2,3} & & & g_{2,m} \\ g_{3,1} & g_{3,2} & g_{3,3} & & \ddots & \\ \vdots & & & \ddots & & \vdots \\ g_{n-1,1} & & \ddots & & g_{n-1,m-1} & g_{n-1,m} \\ g_{n,1} & g_{n,2} & \cdots & & g_{n,m-1} & g_{n,m} \end{bmatrix} \begin{bmatrix} -1 & 0 & & \cdots & & 0 \\ 1 & -1 & 0 & & & \\ 0 & 1 & -1 & 0 & & \vdots \\ & \ddots & \ddots & \ddots & \ddots & \\ \vdots & & 0 & 1 & -1 & 0 \\ 0 & & \cdots & 0 & 1 & 0 \end{bmatrix}$$

$$= \begin{bmatrix} g_{1,2}-g_{1,1} & g_{1,3}-g_{1,2} & g_{1,4}-g_{1,3} & \cdots & g_{1,m}-g_{1,m-1} & 0 \\ g_{2,2}-g_{2,1} & g_{2,3}-g_{2,2} & g_{2,4}-g_{2,3} & & & \\ g_{3,2}-g_{3,1} & g_{3,3}-g_{3,2} & g_{3,4}-g_{3,3} & & \ddots & \vdots \\ \vdots & & & \ddots & & \\ g_{n-1,2}-g_{n-1,1} & & & \ddots & g_{n-1,m}-g_{n-1,m-1} & 0 \\ g_{n,2}-g_{n,1} & g_{n,3}-g_{n,2} & \cdots & \cdots & g_{n,m}-g_{n,m-1} & 0 \end{bmatrix} \quad (1)$$

where the separation distances between every pixel are all equal. The element g_{ij} means the intensity of green color for each pixel, where i and j stand for row and column indices. Eq. (1) leads to find the values of each slope between pixels, and then the maximum point of $\boldsymbol{G}'_{\mathrm{z}}$ is the start point and its minimum point is the end point of the streak, respectively.

Since the noises produce an unwanted distortion in the image, the elimination of local noise points is really necessary. The local matrix $\boldsymbol{G}'_{L(ij)}$ including nine elements for a specified point g'_{ij} can be expressed as

$$\boldsymbol{G}'_{L(ij)} = \begin{bmatrix} g'_{(i-1)(j-1)} & g'_{(i-1)j} & g'_{(i-1)(j+1)} \\ g'_{i(j-1)} & g'_{ij} & g'_{i(j+1)} \\ g'_{(i+1)(j-1)} & g'_{(i+1)j} & g'_{(i+1)(j+1)} \end{bmatrix}. \quad (2)$$

Then, a new noise-reduced point $g'_{N(ij)}$ is obtained by estimating the mean value around the point g'_{ij}, as follows

$$g'_{N(ij)} = \frac{1}{9} \sum_{a=i-1}^{i+1} \sum_{b=j-1}^{j+1} g'_{ab}. \quad (3)$$

This procedure for the minimization of noises is repeating until the criteria on the quality of the streak image should be satisfied.

After completing the formulation of new noise-reduced matrix $\boldsymbol{G}'_{\mathrm{N,z}}$, the streak length can be calculated by determining the maximum point $g_{\max}$ as well as the minimum point $g_{\min}$. Note that these points do not correspond to a center of the particle, so a diameter of particle d_{p} should be subtracted from the streak length. Hence, the particle velocity in z-direction is estimated as follows

$$v_{\mathrm{z}} = \frac{(g_{\min} - g_{\max})\,\gamma - d_{\mathrm{p}}}{t_{\mathrm{E}}} \quad (4)$$

where γ is the ratio of the real distance to the number of pixels, and t_{E} is the exposure time for the streak image of the particle.

3. Experiments

3.1. PDMS-glass microfluidic chip fabrication

Microfabrication procedures are employed to prepare the microfluidic chip using molded PDMS and glass coverslip. We designed the microchannel with a computer-aided design program (Autodesk AutoCAD 2002, CA) and prepared a high-resolution chromium mask supplied by photomask manufacturer (Advance Reproductions Corporation, MA) to minimize the surface roughness of the channel. The microchannel is a slit 3 cm long by 90 μm wide and 1000 μm depth. The master is generated with a negative-tone UV photoresist (MicroChem Corporation, SU8-50, MA) on a silicon wafer (LG-Siltron Inc., 4″ Prime P-100, Korea). The photoresist is spin-coated on a pretreated wafer, which is subjected to a Piranha cleaning. The spin speed of 1150 rpm for a total of 30 s is set to obtain the 90 μm height, which becomes the channel width later.

After the photoresist has been applied to the substrate, it is soft baked on a hot plate. The bake consists of the pre-bake at 65 °C for 5 min and the soft-bake at 95 °C for 20 min. Then, the negatively-patterned photoresist is obtained through the UV exposure with aligner (Karl Suss MA6, Germany), where the power of 17 mW/cm^2 is applied with wavelength of 365 nm (i-line). Following exposure, a post exposure bake (PEB) is performed to selectively cross-link the exposed portions of the mask. The PEB also has a two-step procedure; the

PEB I at 65 °C for 1 min and the PEB II at 95 °C for 4 min. We have the wafer cool down slowly to room temperature to prevent rapid thermal stress, and unexposed photoresist is removed by dissolving with the developer (MicroChem SU8 Developer, MA) for 10 min with mild shaking. After rinsed the wafer with isopropyl alcohol and deionized-water, a master mold containing negatively-patterned photoresist is remained. All the procedures were carried out at the Micro-Nano Fabrication Center located in the Korea Institute of Science and Technology (KIST).

The lateral side of the replica becomes a lid of the slit-like channel, where the thickness of the lid is desirably less than 1 mm to permit optical access for flow imaging. The edge of the wafer mold should be cut and a side wall stands at the cutting surface. To produce a replica, PDMS (Sylgard 184, Dow Corning, MI) is mixed with the curing agent in the volume ratio of 10:1, and poured on the wafer mold [12]. In this study, preliminary tubing is adhered to and stand at the corresponding inlet and outlet reservoirs of 1.2 mm diameter in the master mold, before the pouring. After bubbles are eliminated at 100 torr for 1 h evacuation, the PDMS is cured at 80 °C for 2 h in 1 atm. The PDMS replica is peeled from the master, and then the replica is washed by sonication together with the glass coverslip (Marienfeld Micro Slides, Germany) using methanol. In final, both surfaces to be sealed each other are activated by O_2 plasma for 1 min applying the reactive ion etching (RIE). It is required to put the activated surface of PDMS onto that of glass for about 2–3 h for stronger adhesion.

3.2. Microflow system

The imaging system and experimental set-up are shown in Fig. 2. The high-aspect-ratio of channel depth H to channel width W makes the one-dimensional flow. Seeding of the flow field was achieved with fluorescent polystyrene latex of radius 1.05 μm (Sigma L-5280, MO). Its density was determined to be 1.003. These particles have an excitation peak of 530 nm and emission peak at 560 nm. Latex colloids were dispersed with extremely dilute concentration of 0.48 ppm. Deionized ultrafiltered water was used (Elgastat Prima RO, UK), and the ionic concentration of suspension was maintained as 1.0 mM KCl electrolyte.

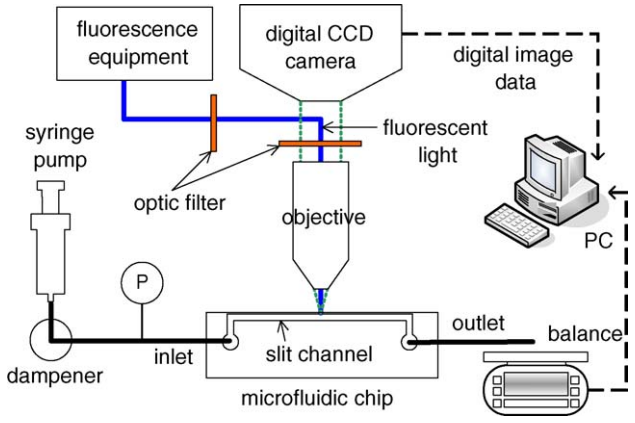

Fig. 2. Schematic of the experimental set-up.

The colloidal suspension was carefully supplied to microfluidic chip by syringe pump (Cole-Parmer 7600 Series, IL) equipped with dampener. A high-precision pressure gauge with ±0.1% FS accuracy (FD2000, Honeywell Sensotec, OH) was connected to a tee to measure the pressure drop across the microchannel. The volumetric flow rate of suspension through the chip was measured by electronic balance (Model AT261, Mettler-Toledo AG, Switzerland) with accuracy of 0.001 g. Both fits and tubing are used with PEEK materials.

3.3. Fluorescent microscope and imaging set-up

The imaging system consisted of stereomicroscope (SV-11, Carl Zeiss, Germany) equipped with fluorescent illuminator. In Fig. 3, it has a zoom range of 0.6× to 6.6× with a numerical aperture of 0.085 and objective lens (Achromat S 2.5×). Illumination was provided by C FL S illuminator having a super-pressure mercury lamp (HBO 103) spectrally filtered with a fluorescent filter cube FITC system. Images were captured using a digital charge-coupled device (CCD) camera (Ultra-High Resolution AxioCam) having a basic resolution of 1300 × 1030 pixels in color, with a digitization of 14 Bit/10 Mhz and a pixel size of 6.7 μm. Its spectral range is 300–1000 nm and the Peltier cooling integrates for up to 40 s.

The focal plane was adjusted to collect the image from the bulk region without the effect of upside wall onto the one-dimensional flow. The image observations were done 1.5 cm downstream of the entrance into the channel where the flow is fully developed. The exposure time was set to 200 ms. The transmitted-light was used to recognize the channel width. However, as it contains a part of band of emission light from the polystyrene latex particles, we depressed the band with red cellophane sheet. With the digital imaging software (AxioVision 3.1, Carl Zeiss), the data from the CCD camera was fed to a monitor for real-time viewing and to a PC-based frame grabber for image acquisition.

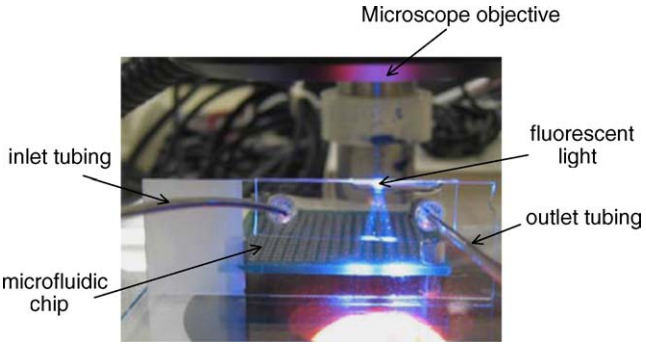

Fig. 3. Photograph of the experimental set-up of PDMS-glass microfluidic chip illuminated by fluorescent light.

4. Results and discussion

4.1. Surface characterization and electric potential estimation

The values of contact angle measured by drop shape measuring system (DSA-10, Krüss GmbH, Hamburg) provide 54° and 98.5° for glass surface and PDMS plate, respectively. The zeta potentials of the materials used in this study were measured with an electrophoretic light scattering spectrophotometer (ELS-8000, Otsuka Electronics, Osaka). As shown in Fig. 4, both the PDMS and the glass surfaces exhibit that the magnitude of the negative zeta potential increases with increasing the pH of suspension. The PDMS plate is negatively charged in above pH 4, but it is considered to be weakly charged as being due to lower magnitude of zeta potential. The glass surfaces are negatively charged likewise the PDMS plate, where its magnitude of zeta potential was greater than that of the PDMS. The zeta potential of the latex colloid was determined using a Zeta-Plus (Brookhaven Instrument Co., NY).

According to the long-range electrostatic interaction energy, both interactions between particle-to-particle and particle-to-wall are important in the microfluidic system [13]. The negative charge of the surface functional group certainly minimizes the affinity of the particles to adhere either to themselves or to the negatively-charged microchannel walls.

The potential profile is obtained applying the finite difference analysis of the electric field along the nonlinear P-B equation. Its dimensionless form for a slit-like channel leads to

$$\frac{d^2\Psi}{dY^2} = (\kappa W)^2 \sinh \Psi \tag{5}$$

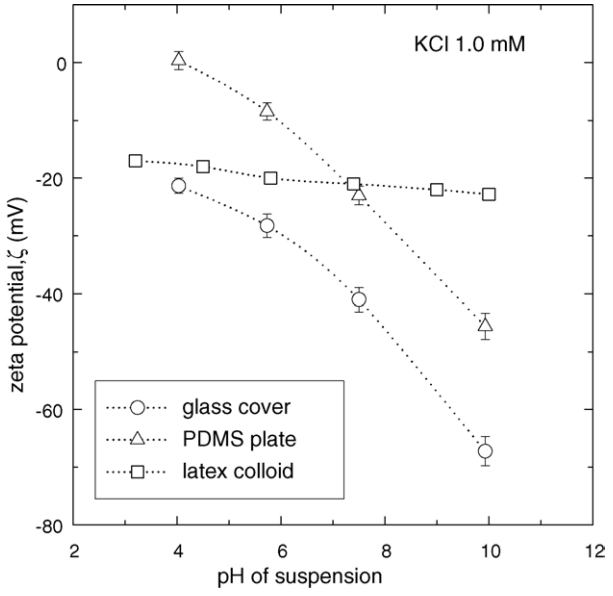

Fig. 4. The zeta potential characterization of seed particle of latex colloid and microfluidic chip materials of PDMS and glass surfaces.

with the dimensionless lateral position Y ($=y/W$) and the dimensionless electric potential Ψ ($=Ze\psi/kT$), where Z is the valence of ions, e the elementary charge, and kT the Boltzmann thermal energy. The inverse electric double layer (EDL) thickness (namely, inverse Debye length) κ is defined by $\sqrt{2n_b Z_i^2 e^2/\varepsilon kT}$, where n_b represents the electrolyte ionic concentration in the bulk solution at the electroneutral state and ε the dielectric constant. The Boltzmann distribution of the ionic concentration of type i (i.e., $n_i = n_b \exp(-Z_i e\psi/kT)$) provides a local charge density $Z_i e n_i$ [14]. The boundary conditions are imposed as $\Psi = \Psi_{s,1}$ at $Y = 0$ and $\Psi = \Psi_{s,2}$ at $Y = 1$. Taking the five-point central difference method yields the left-hand side of Eq. (5) as

$$\frac{d^2\Psi}{dY^2} = \frac{\Psi_{j+1}^{k+1} - 2\Psi_j^{k+1} + \Psi_{j-1}^{k+1}}{\Delta Y^2} \tag{6}$$

where k means the iteration index and the grid index $j = 1, 2, \ldots, N$. The function on the right-hand side of Eq. (5) is linearized as

$$\sinh \Psi = \sinh \Psi_j^k + (\Psi_j^{k+1} - \Psi_j^k) \cosh \Psi_j^k. \tag{7}$$

The finite difference equation obtained from Eqs. (6) and (7) can be solved for Ψ_j^{k+1} by successive iterative calculation, using the value of Ψ obtained in the k-th iteration. Detailed procedure is analogous to the scheme presented in the literature [15]. Once the electric potential Ψ is obtained, it is straightforward to determine the net charge density (i.e., $\Sigma_i Z_i e n_i = Ze(n_+ - n_-)$).

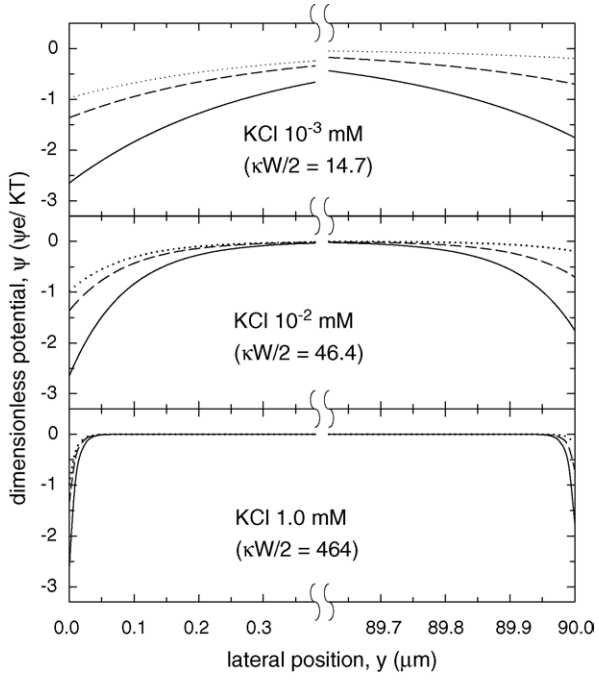

Fig. 5. Electric potential profile in slit-like channel of PDMS-glass microfluidic chip with different suspension pH for KCl 10^{-3}, 10^{-2}, and 1.0 mM; dotted curve (pH 5.0), dashed curve (pH 6.8), solid curve (pH 9.8).

In Fig. 5, getting far from the surface of the channel wall, the electric potential nondimensionalized with kT/e is decreased. Each surface potential is identical to the zeta potential. A decrease of KCl electrolyte concentration corresponds to an increase of the EDL thickness κ^{-1}. The ionic concentration of 1.0 mM KCl is estimated as κ^{-1} of 9.7 nm at 25 °C, since κ^{-1} (nm) is given by [ionic concentration (M)]$^{-1/2}$/3.278 for 1:1 type electrolyte. Fig. 5 exhibits obviously that the EDL thickness of 1.0 mM KCl is very thin compared to the channel width. In this case, we expect both the EDL and the pH of suspension do not exhibit any effects on the flow pattern.

4.2. Particle streak imaging

The flowing from the syringe pump was maintained a constant pressure drop during the experiments. In order to determine the streak length from the acquired digital images, we follow the procedures described in Section 2. First, we select a part of appropriate streak image from the raw streak image, for which the streak image should be cut from the channel wall so as to address the lateral position of a particle. From a streak image of the selected particle with respect to green color component displayed in Fig. 6a, the intensity profile of green color can be obtained as Fig. 6b. Next step is the differentiation of the image matrix in the flow direction of particle by Eq. (1), and then the streak intensity profile is obtained as given in Fig. 6c. In consequence, the local noises are effectively eliminated applying Eqs. (2) and (3) as given in Fig. 6d, from which the local particle velocity is estimated. Above procedure was accomplished by the image processing algorithm developed in this study with implementing MATLAB (Mathworks, MA).

4.3. Velocity profile of dilute suspension

We measured the particle velocities at each position with the method explained previously. In order to guarantee the

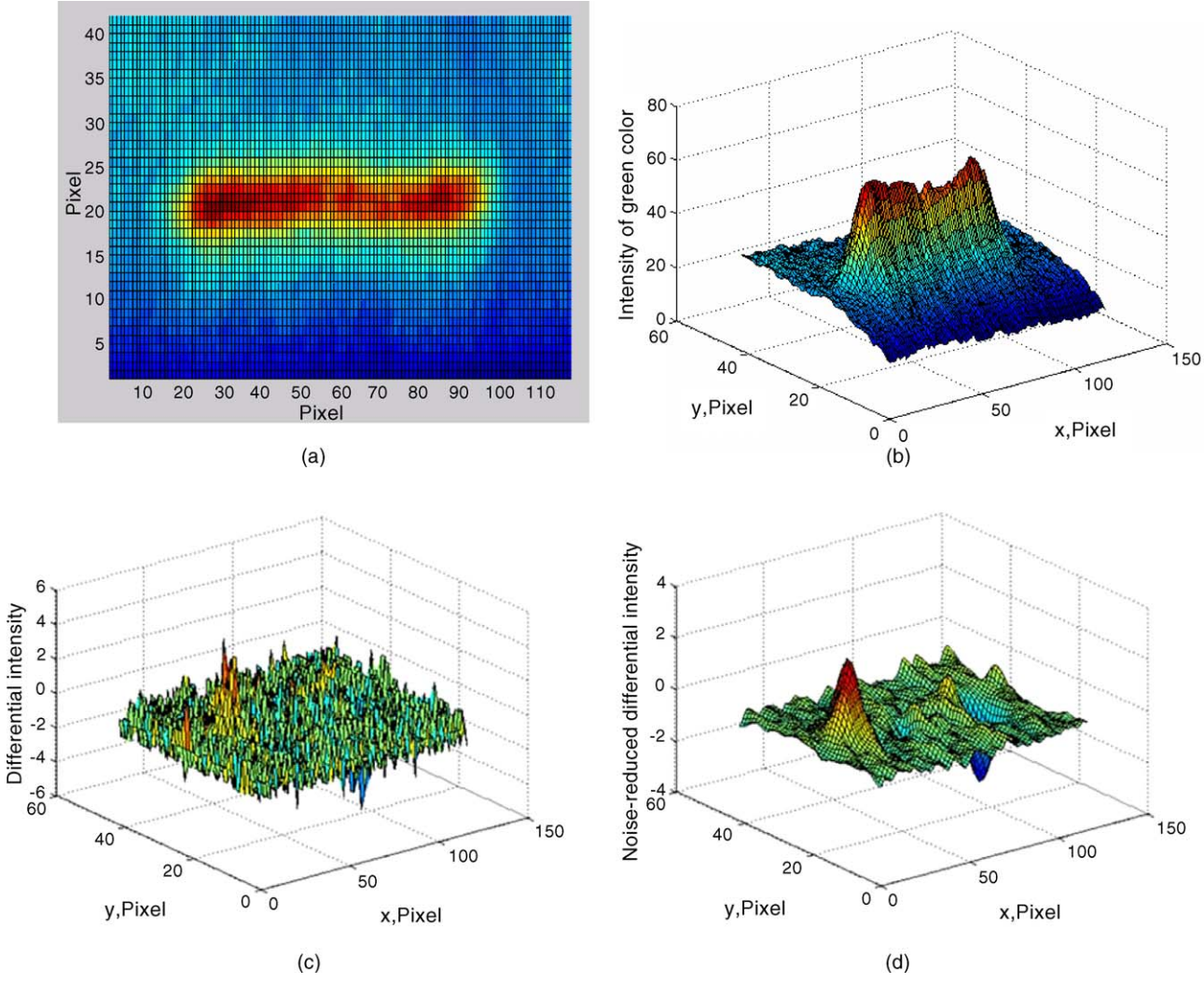

Fig. 6. (a) A selected particle streak image with green color component; (b) intensity profile of green color; (c) differential intensity profile of streak; and (d) differential intensity profile without local noises.

velocity profile of suspension determined by local particle velocities, the ratio of particle diameter d_p to channel width W should be small besides the condition of sufficiently dilute particle concentration. When the latex particle is suspended in a viscous fluid undergoing Poiseuille flow within the channel, both the particle slip velocity and the lateral migration velocity are inevitably presented. A buoyant particle is carried by a velocity less than unperturbed fluid velocity occurred by the particle slip phenomena [16,17]. The migration velocity is related to the hydrodynamic lateral force due to the particle inertia in bounded flows [17,18]. We have performed theoretical calculations conducting relevant equations reported in the literature. As the relative particle size decreases, both the particle slip and the lateral migration effects become almost disappeared. It is emphasized that the value of d_p/W in this study (i.e., 0.023) is consistent with a regime neglecting these effects.

Fig. 7 shows the velocity profile obtained for different pH, meaning a change in the surface potentials of each channel wall as provided in Fig. 4. Even though scatters are shown, the measured velocity profile is well represented by a parabola. The glass wall corresponds to the left-side of x-axis and the PDMS wall corresponds to the right-side of x-axis. We found it is difficult to obtain reliable measurements closer to the wall because of the image noise associated with particle light scatter at the wall surface. Nonetheless, it is clearly recognized that a slip effect exists at the PDMS wall. Instead of the bonding with the glass cover, another type of microfluidic chip having PDMS-PDMS channel was also fabricated in this study. As shown in Fig. 8, the measured velocity profile is represented by the slip velocity at both sides of the wall, allowing a symmetric view.

When the EDL thickness is thin compared to the particle radius, the electrophoretic velocity of a single particle

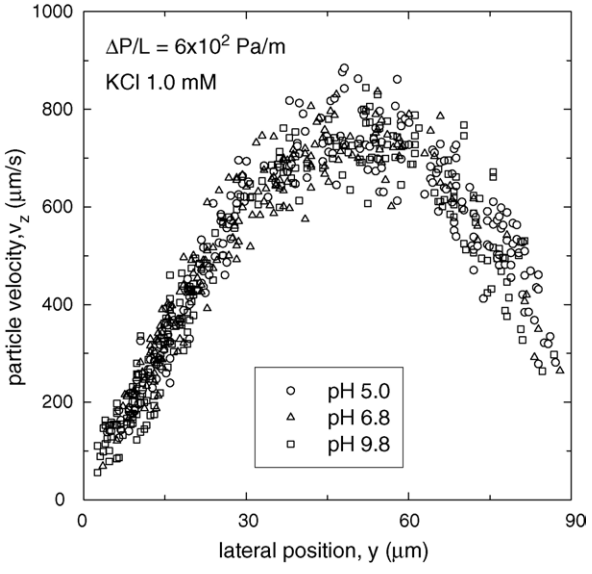

Fig. 7. Velocity profile in slit-like channel of PDMS-glass microfluidic chip for different suspension pH.

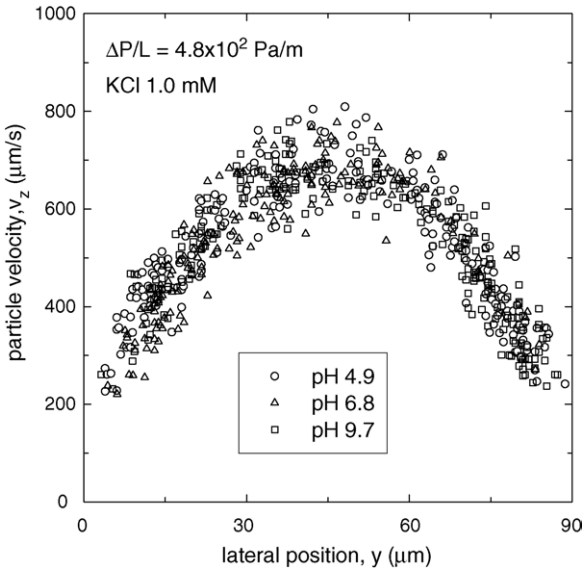

Fig. 8. Velocity profile in slit-like channel of PDMS-PDMS microfluidic chip for different suspension pH.

is obtained as $\varepsilon\zeta_p E_z/\eta$, where ζ_p is the zeta potential of the particle, η the fluid viscosity, and E_z ($=\Delta\phi/L$) the uniform applied electric field along the channel length L [19]. The ϕ is the flow-induced streaming potential in this study, which has quite small order of magnitude compared to the voltages supplied by external power source. Accordingly, it is true that the effect of electrophoretic particle velocity is really negligible in our system.

In order to verify the reliability of the velocity profile determined by the flow imaging, the volumetric flow rate has been measured by the weighing method and then compared with the volumetric flow rate obtained from the regressions on the velocity profile. Fig. 9 shows that the discrepancy between the two results is estimated less than 4% of that obtained by the weighing method. It appears that the flow rate in the PDMS-glass channel has a decreasing trend with increasing pH.

4.4. Slip length

The slip boundary condition at the hydrophobic surface is commonly defined as [20]

$$v_z|_{\text{wall}} = \pm\beta \left.\frac{\partial v_z}{\partial y}\right|_{\text{wall}} \tag{8}$$

where β is assumed to be a material parameter termed the slip length or slip coefficient. This is the equivalent distance below the solid surface at which the no-slip boundary condition would be satisfied if the flow field were extended. Once the channel wall is uncharged (i.e., inert), the velocity profile containing slip effect can be analytically determined from the equation of motion given by $\eta\nabla^2\boldsymbol{v} = \nabla P$. In case of the PDMS-glass microchannel, the analytical solution is derived

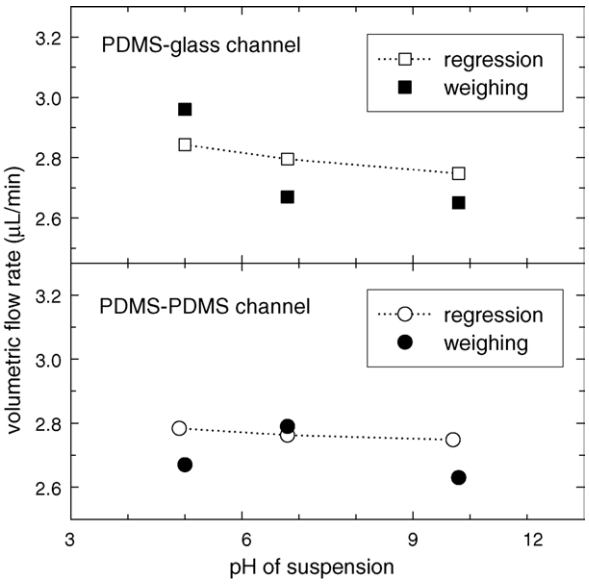

Fig. 9. Comparison of volumetric flow rates determined by polynomial regression and corresponding result by measurements for PDMS-glass channel ($\Delta P/L = 6 \times 10^2$ Pa/m) and PDMS-PDMS channel ($\Delta P/L = 4.8 \times 10^2$ Pa/m).

applying the boundary conditions, viz. $v_z(0) = 0$ at glass wall ($y = 0$) and $v_z(W) = \beta(\mathrm{d}v_z/\mathrm{d}y)|_{y=W}$ at PDMS wall ($y = W$), as follows:

$$v_z(y) = \frac{\Delta P\, W^2}{2\eta L}\left[\left(\frac{W+2\beta}{W+\beta}\right)\left(\frac{y}{W}\right) - \left(\frac{y}{W}\right)^2\right]. \quad (9)$$

The velocity profile in PDMS-PDMS microchannel is determined with $v_z(0) = \beta(\mathrm{d}v_z/\mathrm{d}y)|_{y=0}$ and $v_z(W) = \beta(\mathrm{d}v_z/\mathrm{d}y)|_{y=W}$, yielding

$$v_z(y) = \frac{\Delta P\, W^2}{2\eta L}\left[\left(\frac{y}{W}\right) - \left(\frac{y}{W}\right)^2 + \left(\frac{\beta}{W}\right)\right]. \quad (10)$$

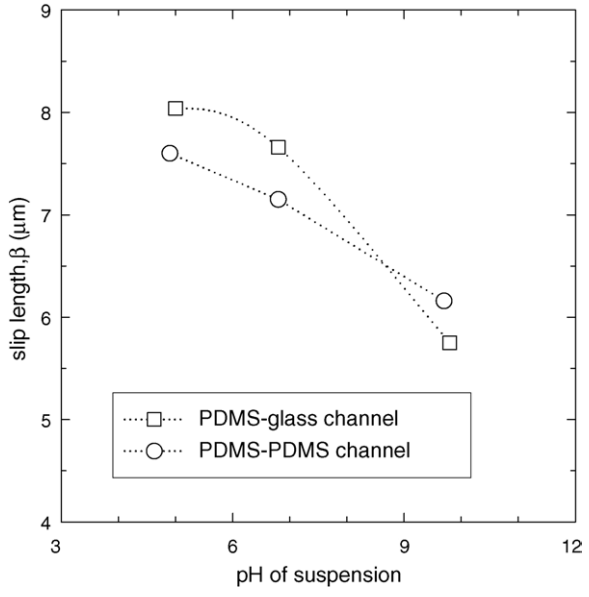

Fig. 10. The variation of the slip length for PDMS-glass and PDMS-PDMS channels.

Eqs. (9) and (10) indicate that, if the slip length β is known, the analytical solution allows us to figure out apparently the reliability of the experimental results. Since the velocity at the solid wall is proportional to the shear rate, it is possible to estimate the slip length analyzing the data points nearby the PDMS wall along the regressions. As shown in Fig. 10, the variations of slip length for both microchannels can be identified ranging about 6–8 μm. The magnitude of β/W ranging 0.06–0.09 is of the order of what is summarized in the literature [21]. Note also that the slip length has an approximate trend to decrease as the pH increases causing the stronger charge effect.

5. Conclusions

Particle streak images are useful in the characterization of microflows since we are able to get velocity profile information. An appropriate methodology based on the streak imaging has been developed and implemented to examine the electrokinetic microflow, which has the advantage of the processing time as well as accuracy.

Applying the fluorescent microscope on a one-dimensional flow field, the velocity profile of dilute latex suspension was obtained in the slit-like channel of PDMS-glass as well as PDMS-PDMS chip. We point out that the ratio of particle size to channel width needs to be small enough to neglect both the particle slip and the lateral migration. The field of view and focus of the microscope were adjusted to collect the image at the focal plane eliminating the effect of upper side onto the one-dimensional flow. The electric potential profile has been computed with variations of the relative EDL thickness to take into account the effect of electrostatic interaction in the microchannel.

The validity of the velocity profile determined by the flow imaging was justified by comparing with the measured flow rate, where a good agreement was found. The Newtonian fluid slip was observed at the hydrophobic surface of the PDMS wall, in which the fluid slip resulted in the increase of flow velocity at a given pressure gradient. From experimental results of velocity profile, it is available to estimate the value of slip length at PDMS wall for different suspension pH. The experiments conducted here and further studies motivate an understanding of the transport in microfluidic system.

Acknowledgements

This work was supported by the Basic Research Funds (R01-2001-000-00411-0 and R01-2004-000-10944-0) from the Korea Science and Engineering Foundations (KOSEF).

References

[1] P.-A. Auroux, D. Iossifidis, D.R. Reyes, A. Manz, Micro total analysis systems. 2. Analytical standard operations and applications, Anal. Chem. 74 (2002) 2637.
[2] H.A. Stone, A.D. Stroock, A. Ajdari, Engineering flows in small devices: microfluidics toward a lab-on-a-chip, Ann. Rev. Fluid Mech. 36 (2004) 381.
[3] R.J. Adrian, Particle-imaging techniques for experimental fluid-mechanics, Ann. Rev. Fluid Mech. 23 (1991) 261.
[4] B. Khalighi, Y.H. Lee, Particle tracking velocimetry: an automatic image processing algorithm, Appl. Optics 28 (1989) 4328.
[5] M. Raffel, C.E. Willert, J. Kompenhans, Particle Image Velocimetry: A Practical Guide, Springer, Berlin, 1998.
[6] S. Devasenathipathy, J.G. Santiago, S.T. Wereley, C.D. Meinhart, K. Takehara, Particle imaging techniques for microfabricated fluidic systems, Exp. Fluids 34 (2003) 504.
[7] J.S. Park, C.K. Choi, K.D. Kihm, Optically sliced micro-PIV using confocal laser scanning microscopy (CLSM), Exp. Fluids 37 (2004) 105.
[8] J.A. Taylor, E.S. Yeung, Imaging of hydrodynamic and electrokinetic flow profiles in capillaries, Anal. Chem. 65 (1993) 2928.
[9] J.P. Brody, P. Yager, R.E. Goldstein, R.H. Austin, Biotechnology at low Reynolds numbers, Biophys. J. 71 (1996) 3430.
[10] T.E. McKnight, C.T. Culbertson, S.C. Jacobson, J.M. Ramsey, Electroosmotically induced hydraulic pumping with integrated electrodes on microfluidic devices, Anal. Chem. 73 (2001) 4045.
[11] M.H. Oddy, J.G. Santiago, J.C. Mikkelsen, Electrokinetic instability micromixing, Anal. Chem. 73 (2001) 5822.
[12] J.C. McDonald, G.M. Whitesides, Poly(dimethylsiloxane) as a material for fabricating microfluidic devices, Acc. Chem. Res. 35 (2002) 491.
[13] M.-S. Chun, W.R. Bowen, Rigorous calculations of linearized Poisson-Boltzmann interaction between dissimilar spherical colloids and osmotic pressure in concentrated dispersions, J. Colloid Interface Sci. 272 (2004) 330.
[14] D. Li, Electro-viscous effects on pressure-driven liquid flow in microchannels, Colloids Surf. A 195 (2001) 35.
[15] M.-S. Chun, T.S. Lee, N.W. Choi, Microfluidic analysis on electrokinetic streaming potential induced by microflows of monovalent electrolyte solution, J. Micromech. Microeng. 15 (2005) 710.
[16] B.P. Ho, L.G. Leal, Inertial migration of rigid spheres in two-dimensional unidirectional flows, J. Fluid Mech. 65 (1974) 365.
[17] J.G. DosRamos, C.A. Silebi, An analysis of the separation of submicron particles by capillary hydrodynamic fractionation (CHDF), J. Colloid Interface Sci. 133 (1989) 302.
[18] R.G. Cox, H. Brenner, The lateral migration of solid particles in Poiseuille flow. I. Theory, Chem. Eng. Sci. 23 (1968) 147.
[19] R.F. Probstein, Physicochemical Hydrodynamics: An Introduction, Wiley, New York, 1994.
[20] D.C. Tretheway, C.D. Meinhart, Apparent fluid slip at hydrophobic microchannel walls, Phys. Fluids 14 (2002) L9.
[21] E. Lauga, H.A. Stone, Effective slip in pressure-driven Stokes flow, J. Fluid Mech. 489 (2003) 55.